10th International Conference on Fracture Mechanics of Concrete and Concrete Structures
FraMCoS-X
G. Pijaudier-Cabot, P. Grassl and C. La Borderie (Eds)
https://doi.org/10.21012/FC10.235577

DETERMINAION OF FRACTURE PARAMETERS OF CORAL AGGREGATE CONCRETE AFTER IMMERSION IN SEAWATER

SHUTONG YANG[*,†], XIANSHUN ZHANG[††] AND WEIYING XU[†††]

[*†]Ocean University of China; Cooperative Innovation Center of Engineering Construction and Safety in Shandong Blue Economic Zone
Qingdao, P.R.China
e-mail: shutongyang2013@163.com

[†] Ocean University of China
Qingdao, P.R.China
e-mail: 799733217@qq.com

†† Ocean University of China
Qingdao, P.R.China
e-mail: 69358889@qq.com

Key words: Fracture parameters, Coral aggregate concrete (CAC), Immersion, Maximum fracture load, boundary effect

Abstract: This paper is mainly concerned with the determination of fracture parameters of coral aggregate concrete (CAC) under different curing ages and conditions by virtue of three-point-bending tests. Four groups of CAC are tested. The first ones were cured for 56 days under standard environment and the second ones were immersed in seawater for 28 days after 28-day curing under standard environment. The third ones were cured for 118 days under standard environment and the fourth ones were immersed in seawater for 90 days after 28-day curing under standard environment. The initial crack length-to-beam depth ratios are set from 0.1 to 0.7 in each group. Results show that the failure modes of all the specimens are coral aggregate fracture without interfacial debonding between the aggregate and surrounding mortar. The maximum fracture load increases with the curing age. Besides, the beams cured by immersion in seawater have higher maximum facture loads compared to those cured under standard environment. Moreover, an analytical approach is proposed to determine the fracture parameters of CAC. The size-independent tensile strength and fracture toughness are obtained based on the boundary effect model by virtue of the experimentally determined maximum fracture loads. The analytically predicted maximum fracture loads are given related to the local fracture energy at the crack-tip region. The local fracture energy distribution and size-independent fracture energy can be obtained by the comparison between the analytical and experimental maximum fracture loads. It is found that the tensile strength increases with the curing age and becomes larger if the specimens were immersed in seawater for curing. But both the fracture toughness and fracture energy seem insensitive to the curing ages and conditions.

1 INTRODUCTION

Construction of islands far away from the mainland has been carried out and developed recently with the rapid development of marine exploitation. Corals can be used as aggregates instead of river sand and crushed stones in

concrete production. It can avoid long distance ship transport of aggregates and fresh water from the mainland and then reduce the construction cost and period. Different from the main mineral components in natural aggregates, coral reefs and sand has large amount of calcium carbonate which takes up more than 96% [1]. Moreover, coral aggregates should be presoaked before mixing concrete due to the porous surface and high water absorption of coral particles [2]. Early strength of coral aggregate concrete (CAC) develops faster due to the chloride effects from the corals compared to ordinary concrete (OC) with the same strength grade [3, 4]. The ratios of 7-day strength to 28-day strength even exceed 80% [5]. Besides, the ratios of uniaxial compressive strength to cubic compressive strength are significantly higher than those in OC [5]. The splitting tensile strength and elastic modulus are larger than those of OC with the same strength because of the better bond performance between the porous coral aggregate and surrounding mortar [3]. However, it is found that CACs have significant brittle properties especially when they are subjected to compression as columns [6, 7]. Therefore, the CAC columns should be enveloped by FRP (fiber-reinforced polymer) tubes to prevent spalling failure [8]. Tan et al. [9] evaluated the compressive strength of CAC by using non-destructive techniques and established the correlation between the compressive strength and ultrasonic pulse velocity. Cheng et al. [10] added fly ash, blast furnace slag and metakaolin instead of part of Portland cement to mix CAC and found that the chloride diffusion coefficient is reduced.

Since the coral aggregates and mixing seawater have high content of chloride ions, steel bars can not be applied in CACs as reinforcements by considering the structural durability. Thus, FRP bars can be adopted due to their high resistance to chloride corrosion. The authors [5] analyzed the bond properties between FRP bars and CAC aimed at the effects of fiber type, surface type, bond length and curing conditions. Wang et al. [11] studied the bond behavior of FRP bars to CAC after immersion in seawater with different immersion days and water temperatures. The bond strength is found to decrease if the seawater has high temperature [11].

Reinforced CAC structures are generally applied in ocean environment. The cracks in CAC should be paid much attention to. Formation of cracks in concrete provides channels for external corrosive ions penetration. Even if FRP bar is used, it will be damaged by hydroxide ions from concrete pore solution transmitted by externally permeating water. Cracks will much affect the durability of concrete structures. Therefore, it is necessary to study the fracture properties of CAC under ocean environment. To our best knowledge, there is no literature aimed at the fracture behavior of CAC so far.

The intention of this paper is to determine the fracture parameters of CAC after immersion in seawater for different days by virtue of three-point-bending tests. Then the CAC beams cured under standard environment are prepared for comparison.

2 EXPERIMENTAL PROGRAMME

2.1 Materials

Cement used in the test is P.O.42.5 ordinary Portland cement (Chinese Standard GB 175 [12]). Both mixing water and curing water are artificial seawater according to the seawater in South China Sea. The detailed chemical components are shown in Table 1. Fig. 1 shows the used coral sand with apparent density, bulk density and water content of 2517 kg/m^3, 1415 kg/m^3, and 11%, respectively. Coarse aggregates used in the test are columnar coral particles with and maximum diameter of 10 mm and porous properties as shown in Fig. 2. The apparent and bulk densities are 1899 kg/m^3 and 918 kg/m^3, respectively. The water content of particles is 15%. Moreover, polycarboxylate-based high-range water reducer (HRWR) was introduced.

Table 1: Chemical components of artificial seawater (g/L)

NaCl	$MgCl_2$	Na_2SO_4	$CaCl_2$	KCl	$NaHCO_3$

22.16	5.265	3.861	1.082	0.745	0.207

Figure 1: Coral sand

Figure 2: Columnar coral particles

2.2 Mix proportion

All the coarse aggregates are immersed in seawater for 24 h before concrete mixing. The detailed mix proportion of CAC is seen in Table 2.

Table 2: Mix proportion of CAC (kg/m^3)

Seawater	Cement	Coral sand	Coral stones	HRWR
190	500	556	712	2.5

The slump values of fresh concrete from different batches are kept between 110 mm and 125 mm.

2.3 Three-point-bending test

All the specimens with sizes of 100×100×515 mm^3 were first cured in standard environment with temperature of 20°C and relative humidity of 95% for 28 days. Then the beams were divided into four groups. The specimens in the first group denoted by Z28 continued to be cured in standard environment for 28 days and the ones in the second group denoted by J28 were immersed in 20°C seawater for 28 days until the test begun. Moreover, the third group denoted by Z90 was kept in the same standard environment for 90 days and the fourth group denoted by J90 was immersed in 20°C seawater for 90 days. In each group, the initial crack length-to-beam depth ratios (a_0/h) are set from 0.1 to 0.7. Four samples are prepared for each ratio. Therefore, there are totally 112 beams to be tested. Moreover, cubic specimens and prisms are made to determine the cubic compressive strength and elastic modulus of CAC in the same condition with the beams in each group, respectively.

The fracture experiment was carried out when the beams were cured at designed age. The test set-up is shown in Fig. 3. The span length L is four times of the beam depth h, i.e., L=4h. The test machine has a maximum range of 2000 kN. In each beam, two strain gauges are set horizontally at the same height with the crack-tip to monitor the initial cracking state. A load cell with the maximum range of 7 kN is adopted to detect the applied load F, and a clip gauge having a maximum range of 4 mm is used to measure the crack mouth opening displacement (*CMOD*). All the readings from the above cells were collected by a data acquisition system. The application of load is controlled by the vertical displacement of loading head and the rate is kept as 0.2 mm/min.

Figure 3: Test set-up

3 RESULTS AND DISCUSSIONS

3.1 Cubic strength and elastic modulus

The cubic strengths f_{cu} and elastic moduli E_c of CAC in the four groups are summarized in Table 3.

Table 3: Cubic strength and elastic modulus of CAC

Nos. of groups	f_{cu} (MPa)	E_c (GPa)
Z28	32.71	21.4
J28	34.08	22.3
Z90	35.9	23.9
J90	36.76	24.5

Apparently, both the f_{cu} and E_c increase with the curing age. The strengths of CAC after seawater immersion are slightly higher than those cured in standard environment. It has been mentioned that all the coral aggregates are presoaked in seawater before mixing concrete. As the curing age increases, the absorbed water in the coral particles is gradually released. It then results in further hydration reaction of surrounding paste. The interface between the coral particles and cement mortar becomes denser. Therefore, the strengths of CAC increase as the curing age is longer. Moreover, the subsequent hydration reaction would be more sufficient under seawater immersion conditions. Thus, the strengths of CACs after seawater immersion would be higher.

3.2 Analysis of crack propagation process

The crack propagation process of CAC is very similar to that of OC. It still includes the initial cracking state, stable crack propagation stage and unstable crack propagation process. The typical variations of the applied load F with *CMOD* in all the four groups are shown in Fig. 4.

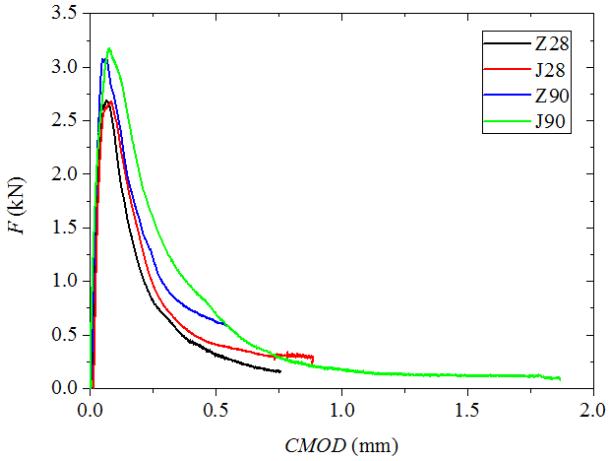

Figure 4: Typical *F-CMOD* curves

Fig. 4 gives the typical *F-CMOD* curves in the four groups with a_0/h=0.3. The maximum fracture load F_{max} increases significantly with the curing age. The F_{max} in the beams after seawater immersion are higher than those in the specimens cured under standard environment. It is also due to the subsequent hydration reaction of cement paste of CAC and more sufficient reaction under seawater immersion condition.

Moreover, the failure modes of all the beams are fracturing of columnar coral aggregates. It is mainly because cement mortar in CAC has good bond performance with coral particles due to the porous properties of the latter. The failure mode tends to be aggregate fracture rather than interfacial debonding. As the curing age increases and the curing condition is changed from standard environment to seawater immersion, the interfacial transition zones become denser.

4 DETERMINATION OF FRACTURE PARAMETERS

Fracture toughness, fracture energy and uniaxial tensile strength are important parameters in describing the crack propagation process of concrete. However, the parameters obtained from test are generally found to be size-dependent. Hu et al. [13-18] presented a boundary effect model (BEM) to explain the mechanisms of size effect which is mainly induced by the interaction between fracture process zone (FPZ) and boundary of specimen. A bi-linear model for local fracture energy distribution was proposed by indicating the back boundary effect and size-independent fracture energy G_F [19]. The authors proposed a maximum fracture load model (MFLM) to correlate the maximum fracture load F_{max} with the local fracture energy at the crack-tip region $g_{f\text{-}tip}$ for concrete [20] and mortar [21]. The local fracture energy distribution indicating both the front and back boundary effects and the G_F are obtained by comparison between the analytical and experimental maximum fracture loads [20, 21]. However, the maximum tensile stress f_{tmax} at the fictitious crack-tip is necessary in the model by the authors [20, 21]. The physical meaning of f_{tmax} is not clear and it may be the true uniaxial tensile strength $f_{t\text{-}in}$ of concrete which is too difficult to be obtained with accuracy in uniaxial tensile test. Recently, Hu et al. [22-24] improved the BEM to predict the size-independent uniaxial tensile strength $f_{i\text{-}in}$ and fracture toughness K_{IC}. If the f_{tmax} in the MFLM is equal to the $f_{i\text{-}in}$ predicted by Hu et al. [22-24], the MFLM can be used more conveniently without pre-estimation of the f_{tmax} which is usually difficult to be estimated especially when new cementitious materials are considered. Thus, the main intention of this section is to clarify the relationship between the $f_{t\text{-}in}$ and f_{tmax} and determine the fracture parameters of CAC by combing the MFLM with the improved BEM.

The analytical approach is proposed for a three-point-bending notched concrete beam as shown in Fig. 3. The width, depth and span length of beam are denoted by b, h and L, respectively, and L=4h. a_0 is used to represent the initial crack length.

4.1 Determination of $f_{t\text{-}in}$

When the maximum fracture load F_{max} is reached, the stress distribution in the cracked section can be assumed as shown in Fig. 5 [22-24]. Herein, the critical crack propagation length is expressed by βd_{max}, and β and d_{max} are a discrete number and maximum diameter of coral aggregates, respectively.

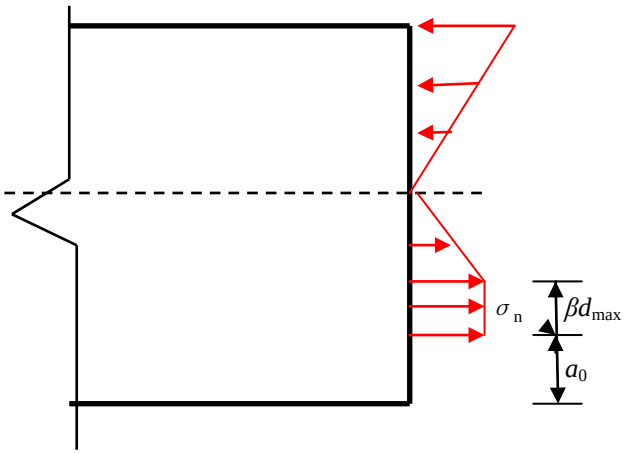

Figure 5: Stress distribution in the cracked section in the ultimate state [22-24]

According to the BEM [13-18], the nominal strength σ_n can be expressed as follows.

$$\sigma_n = \frac{f_{t-in}}{\sqrt{1+\frac{a_e}{a_\infty^*}}} \tag{1}$$

$$a_e = \left(\frac{(1-\alpha)^2 Y(\alpha)}{1.12}\right)^2 \cdot a_0 \tag{2}$$

$$\alpha = \frac{a_0}{h} \tag{3}$$

$$Y(\alpha) = \frac{1.99-\alpha(1-\alpha)(2.15-3.93\alpha+2.7\alpha^2)}{\sqrt{\pi}(1+2\alpha)(1-\alpha)^{3/2}} \tag{4}$$

$$a_\infty^* = 0.25\left(\frac{K_{IC}}{f_{t-in}}\right)^2 \tag{5}$$

It can be rearranged as follows.

$$\frac{1}{\sigma_n^2}=\frac{1}{f_{t-in}^2}+\frac{4}{K_{IC}^2}a_e \tag{6}$$

The relationship between the F_{max} and σ_n can be given by virtue of the equilibrium conditions of forces in Fig. 5, i.e.,

$$\sigma_n=\frac{(6F_{max}+3W)L}{4b(h-a_0)(h-a_0+2\beta d_{max})} \tag{7}$$

Because of coarse structure in concrete, the discrete number β in Eq. (7) is uncertain. For the beams with h/d_{max}<30, the β should be 1~1.5 [20, 21] and β=1 can give the best estimation [24]. Therefore, β=1 is also adopted in the present study.

Once the values of a_0 (varying in a wide range) and the corresponding F_{max} are collected from the test, a series of scattered points indicating the variation $1/\sigma_n^2$ of with a_e will be given. A linear equation of $1/\sigma_n^2$ related to a_e can be yielded based on the linear regression method. The values of K_{IC} and $f_{t\text{-}in}$ are then determined from the slope and intercept of the fitted curve. The results of K_{IC} and $f_{t\text{-}in}$ in the four groups are shown in Fig. 6 as follows.

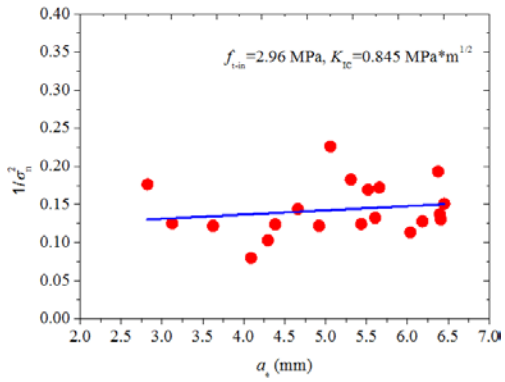

(a)

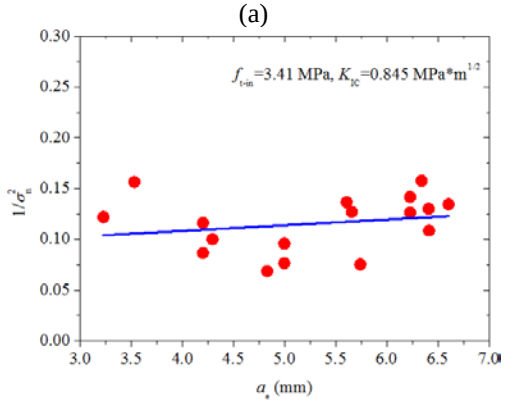

(b)

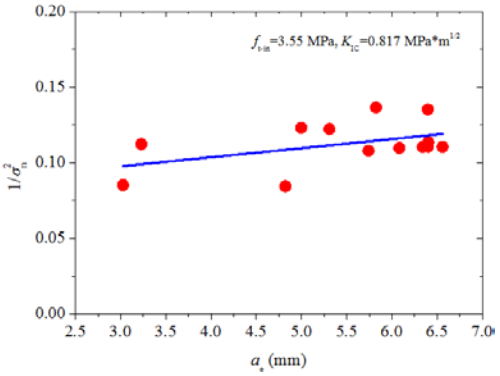

(c)

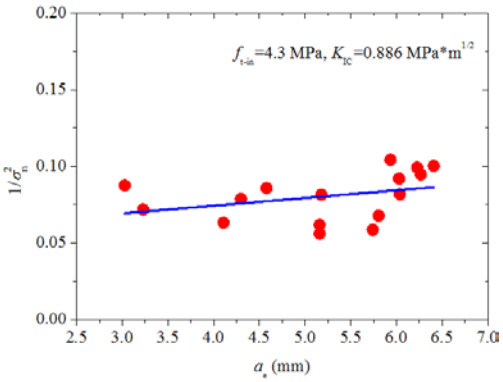

(d)

Figure 6: Determination of $f_{t\text{-}in}$ and K_{IC}

It can be seen that the $f_{t\text{-}in}$ increases with the increasing of curing age. Moreover, the $f_{t\text{-}in}$ shows an increase after the beams were immersed in seawater. As the curing age becomes longer, the hydration reaction is more sufficient accompied by subsequent hydration reaction due to the water release from the porous coral aggregates. The reaction developes more sufficiently after the seawater immersion. It then results in higher values of $f_{t\text{-}in}$ at higher curing ages or cured in seawater. However, the K_{IC} seems insensitive to the curing age and condition. The reason can be explained as follows. The K_{IC} depends on both the tensile strength and deformability of concrete. As the curing age increases or curing condition is changed from standard enviornment to seawater immersion, further hydration reaction is sufficient especially for the paste surrounding coral particles. The fracture resistance of cement mortar and bond action between the mortar and coral aggregates become so strong that the deformability of resulting concrete is reduced. Therefore, although the $f_{t\text{-}in}$ shows a certain increase if the

curing age becomes longer or the specimens are cured in seawater, the variation of K_{IC} is marginal.

4.2 Determination of G_F

The present section is concerned with the determination of local fracture energy distribution and size-independent fracture energy based on the MFLM [20, 21]. Since the $f_{t\text{-}in}$ is obtained above, it may be the f_{tmax} in the MFLM. It is assumed that the two parameters are equal and then the f_{tmax} is replaced by the $f_{t\text{-}in}$ in the present study. The validity of the assumption will be verfied later. After the initial cracking state, the stress distribution in the cracked section is shown in Fig. 7 as follows.

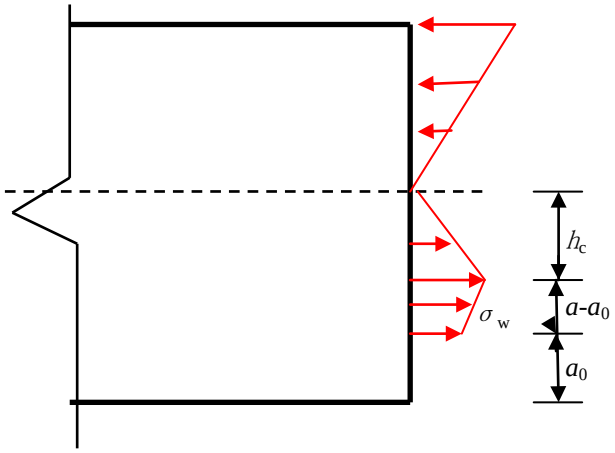

Figure 7: Stress distribution in the cracked section

The relationship between the cohesive stress σ_w and crack opening width w is simplfied by a bi-linear model [25] as shown in Fig. 8. It reads

$$\sigma_w = f_{t-in}\left(1-\frac{28 f_{t-in}}{25 g_f} w\right) \quad \left(0 \le w \le \frac{5 g_f}{7 f_{t-in}}\right) \tag{8}$$

$$\sigma_w = \frac{9}{40} f_{t-in}\left(1-\frac{7 f_{t-in}}{45 g_f} w\right) \left(\frac{5 g_f}{7 f_{t-in}} \le w \le \frac{45 g_f}{7 f_{t-in}}\right) \tag{9}$$

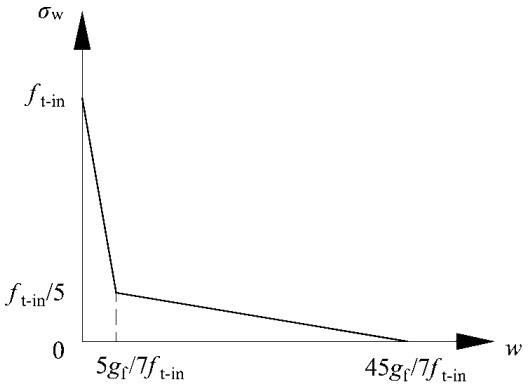

Figure 8: Bilinear model for the σ_w-w relationship

The area under the bilinear curve is local fracture energy g_f.

The values of g_f in the fictitious crack region are assumed constant as the $g_{f\text{-}tip}$. According to the equlibrium condition of forces in the cracked section in Fig. 7, the h_c is given by

$$h_c = \frac{(h-a)^2}{2(h-a)+2(a-a_0)(1-14 f_{t-in} w_t / 25 g_{f-tip})} \tag{10}$$

The bending moment M can be expressed as a funtion of equivalent crack length a and crack-tip opening displacement w_t, and denoted by

$$M = f_M(a, w_t) \tag{11}$$

By introducing a compatibility equation of *CMOD* related to M and a by Tada et al. [26], an equilibrium equation of a and w_t can be given by

$$f_1(a, w_t) = 0 \tag{12}$$

To seek the maximum value M_{max} of M, a Lagrange function $\Phi(a, w_t, \lambda)$ is established as follows.

$$\Phi(a, w_t, \lambda) = f_M(a, w_t) + \lambda \times f_1(a, w_t) \tag{13}$$

By solving the following equation

$$\frac{\partial \Phi}{\partial a} = \frac{\partial \Phi}{\partial w_t} = \frac{\partial \Phi}{\partial \lambda} = 0 \tag{14}$$

The critical crack length a_c and critical crack-tip opening width w_{tc} are yielded. The M_{max} is then obtained by inserting a_c and w_{tc} into Eq. (11). The F_{max} can be given by

$$F_{max} = \frac{4 M_{max}}{L} - \frac{W}{2} \tag{15}$$

According to the MFLM, the F_{max} is much related to the $f_{t\text{-}in}$ and the $g_{f\text{-}tip}$. The former has been predicted based on the improved BEM

[22-24]. Only the $g_{f\text{-}tip}$ needs to be estimated by virtue of the comparison between the analytical F_{max} and experimental ones. Moreover, since the values of K_{IC} in the four groups are close to each other, the $g_{f\text{-}tip}$ can be adopted as the same value, i.e., 100 N/m. Then the comparisons between the analytical and experimental results are shown in Fig. 9 as follows.

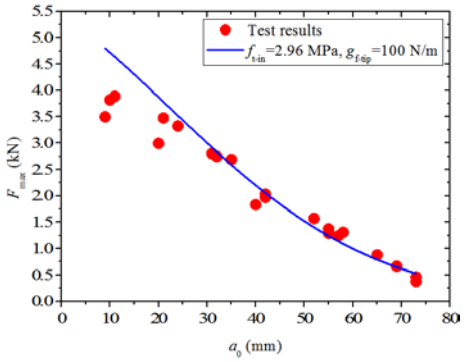

(a)

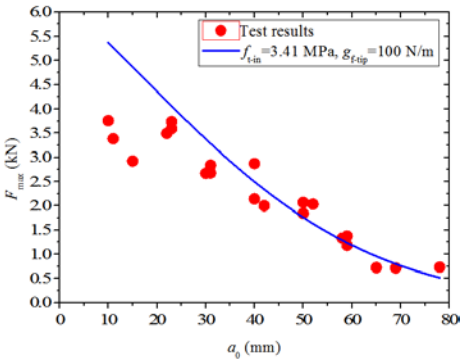

(b)

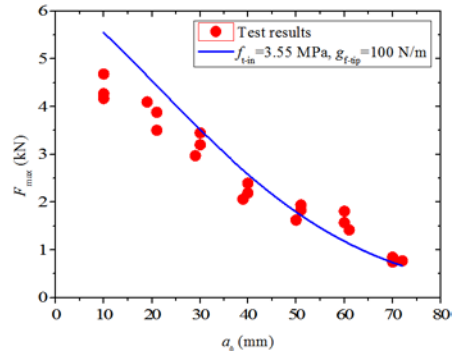

(c)

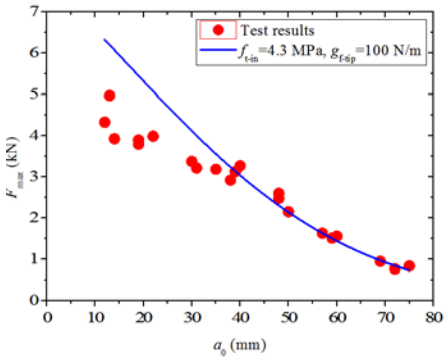

(d)

Figure 9: Comparison between the analytical and experimental results

In each group, when the a_0 is longer than 30 mm (=3d_{max}), the scattered points from the test almost distribute symmetrically along the solid line and more than 80% of the points even touch the line. It means the analytically prediced F_{max} show very good aggrement with the experimentally determined ones for the beams with a_0>30 mm. The predicted values of $f_{t\text{-}in}$ and the estimated values of $g_{f\text{-}tip}$ prove to be reasonable and the $f_{t\text{-}in}$ is actually the maximum tensile stress f_{tmax} at the fictitious crack-tip. When the a_0 is shorter than 30 mm or 3d_{max}, the crack-tip is near the front boundary of specimen and the overestimation of F_{max} is because the actual values of $g_{f\text{-}tip}$ are lower than 100 N/m due to the front boundary effect as indicated by the authors [20, 21]. In other words, the transition length L_{lf} induced by the front boundary effect should be about 3d_{max}. Moreover, the transition length L_{lb} induced by the back boundary effect is equal to L_{lf} or 3d_{max}. But the largest values of a_0 in all the four groups are around 70 mm with the remained ligament lengths of 30 mm (=3d_{max}). Therefore, the back boundary effect is insignificant in the present study. The values of $g_{f\text{-}tip}$ in the regions of 30 mm<a_0<70 mm should be the size-independent fracture energy G_F which is affected by neither front nor back boundary effect. In the present study, the G_F is 100 N/m irrelevant to the curing age and condition.

The fracture parameters of CAC under different curing ages and conditions are summarized in Table 4 as follows.

Table 4: Fracture parameters of CAC

Nos. of groups	$f_{t\text{-}in}$ (MPa)	K_{IC} (MPa·√m)	G_F (N/m)
Z28	2.96	0.845	100
J28	3.41	0.845	100
Z90	3.55	0.817	100
J90	4.3	0.886	100

5 CONCLUSIONS

The present study analyzed fracture properties of CAC after seawater immersion at different curing ages by virtue of three-point-bending tests. Four groups of beams were prepared by indicating two curing ages, i.e., 56 days and 118 days, and two curing conditions, i.e., standard environment and seawater immersion. The size-independent uniaxial tensile strength $f_{t\text{-}in}$ and fracture toughness K_{IC} are predicted based on the improved BEM [22-24]. The local fracture energy distribution and size-independent fracture energy G_F are obtained based on the MFLM [20, 21] by introducing the predicted $f_{t\text{-}in}$. The conclusions are drawn as follows.

1. The maximum tensile stress at the fictitious crack-tip is actually the $f_{t\text{-}in}$ which can be predicted from the improved BEM.
2. As the curing age increases, the $f_{t\text{-}in}$ of CAC becomes larger due to the further hydration reaction of paste surrounding coral aggregates. The beams after seawater immersion have larger $f_{t\text{-}in}$ compared to those cured under standard environment.
3. Both the K_{IC} and G_F seem insensitive to the curing age and condition.

ACKNOWLEDGEMENT

The authors gratefully acknowledge funding from the National Natural Science Foundation of China (Grant 51778591) and Educational Innovation and Research Foundation of Graduate Student in Shandong Province of China (Grant HDJG17006).

REFERENCES

[1] Chen, Z.L., Sun, G.F., Tang, X.N., Liu, Y.L., 2008. Study on applications of concrete from coral reef sand mixed with seawater for patching-up in reef engineering. *Coast. Engng.* 27(4): 60-69. (in Chinese)

[2] Arumugam, R.A., Ramamurthy, K., 1996. Study of compressive strength characteristic of coral aggregate concrete. *Mag. Concr. Res.* 48(176): 141-148.

[3] Wang, L., Fan, L., 2015. Analysis of strength properties and failure modes of coral aggregate concrete. *China Concr. Cem. Prod.* (1): 1-4. (in Chinese)

[4] Zhao, Y.L., Han, C., Zhang, S.Z., Ge, R.D., 2011. Experimental study on the compression age strength of seawater coral concrete. *Concr.* (256): 43-45. (in Chinese)

[5] Yang, S.T., Yang C., Huang, M.L., Liu, Y., Jiang, J.T., Fan, G.X., 2018. Study on bond performance between FRP bars and seawater coral aggregate concrete. *Constr. Build. Mater.* 173: 272-288.

[6] Da, B., Yu, H. F., Ma, H. Y., Tan, Y. S., Mi, R. J., Dou, X. M. 2016. Experimental investigation of whole stress-strain curves of coral concrete. *Const. Build. Mater.* 122: 81-89.

[7] Da, B., Yu, H.F., Ma, H.Y., Wu, Z.Y.,2018. Research on compression behavior of coral aggregate reinforced concrete columns under large eccentric compression loading. *Ocean Engng.* 155:251-260.

[8] Wang, J., Feng, P., Hao, T.Y., Yue, Q.R.,2017. Axial compressive behavior of seawater coral aggregate concrete-filled FRP tubes. *Constr. Build. Mater.* 147: 272-285.

[9] Tan, Y.S., Yu, H.F., Mi, R.J., Zhang, Y.,2018. Compressive strength evaluation of coral aggregates seawater concrete (CAC) by non-destructive techniques. Engng. Struct. 176: 293-306.

[10] Cheng, S.K., Shui, Z.H., Sun, T., Yu, R., Zhang, G.Z., Ding, S., 2017. Effects of fly ash, blast furnace slag and metakaolin on mechanical properties and durability of coral sand concrete. *Appl. Clay Sci.* 141: 111-117.

[11] Wang, L., Mao, Y.D., Lv, H.B., Chen, S., Li, Wei., 2018. Bond properties between FRP bars and coral concrete under seawater conditions at 30, 60, and 80 °C. *Constr. Build. Mater.* 162: 442-449.

[12] CS (Chinese Standard) GB 175. Common Portland cement. General Administration of Quality Supervision. China: Quality Supervision Inspection and Quarantine of the People's Republic of China and National Standardizing Committee of the People's Republic of China; 2007 (in Chinese).
[13] Hu, X.Z., Wittmann, F.H., 1992. Fracture energy and fracture process zone. *Mater. Struct.* 25(6): 319-326.
[14] Hu, X.Z., Wittmann, F.H., 2000. Size effect on toughness induced by crack close to free surface. *Engng. Fract. Mech.* 65(2): 209-221.
[15] Hu, X.Z., 2002. An asymptotic approach to size effect on fracture toughness and fracture energy of composites. *Engng. Fract. Mech.* 69(5): 555-564.
[16] Hu, X.Z., Duan, K., 2004. Influence of fracture process zone height on fracture energy of concrete. *Cem. Concr. Res.* 34(8): 1321-1330.
[17] Hu, X.Z., Duan, K., 2007. Size effect: Influence of proximity of fracture process zone to specimen boundary. *Engng. Fract. Mech.* 74: 1093-1100.
[18] Hu, X.Z., Duan, K., 2008. Size effect and quasi-brittle fracture: the role of FPZ. *Int. J. Fract.* 154(1–2): 3-14.
[19] Duan, K., Hu, X.Z., Wittmann, F.H., 2003. Boundary effect on concrete fracture and non-constant fracture energy distribution. *Engng. Fract. Mech.* 70(16): 2257-2268.
[20] Yang, S.T., Hu, X.Z., Wu, Z.M., 2011. Influence of local fracture energy distribution on maximum fracture load of three-point-bending notched concrete beams. *Engng. Fract. Mech.* 78(18),: 3289–3299.
[21] Yang, S.T., Hu, X.Z., Leng, K.Z., Liu, Y.L., 2014. Correlation between cohesive crack-tip local fracture energy and peak load in mortar specimens. *J. Mater. Civ. Engng.* 10.1061/(ASCE)MT.1943-5533.0000959 26(10): 04014069.
[22] Wang, Y.S., Hu, X.Z., Liang, L., Zhu, W.C., 2016. Determination of tensile strength and fracture toughness of concrete using notched 3-p-b specimens. *Engng. Fract. Mech.* 160: 67-77.
[23] Wang, Y.S., Hu, X.Z., 2017. Determination of tensile strength and fracture toughness of granite using notched three-point-bend samples. *Rock. Mech. Rock. Engng.* 50(1): 17-28.
[24] Hu, X.Z., Guan, J.F., Wang, Y.S., Keating, A., Yang, S.T., 2017. Comparison of boundary and size effect models based on new developments. *Engng. Fract. Mech.* 175: 146-167.
[25] Abdalla, H.M., Karihaloo, B.L., 2004. A method for constructing the bilinear tension softening diagram of concrete corresponding to its true fracture energy. *Mag. Concr. Res.* 56(10): 597-604.
[26] Tada, H., Paris, P. C., Irwin, G. R., 1985. *The stress analysis of cracks handbook*, Paris Productions, St. Louis, MO.